Actin Binding of Ezrin Is Activated by Specific Recognition of PIP_2-Functionalized Lipid Bilayers[†]

Matthias Janke,[‡] Alexander Herrig,[§] Judith Austermann,[||] Volker Gerke,[||] Claudia Steinem,[§] and Andreas Janshoff*[,‡]

Institute of Physical Chemistry, University of Mainz, Welder Weg 11, 55128 Mainz, Germany, Institute of Organic and Biomolecular Chemistry, Georg-August-University of Göttingen, Tammannstrasse 2, 37077 Göttingen, Germany, and Institute of Medical Biochemistry, ZMBE, University of Münster, von-Esmarch-Strasse 56, 48149 Münster, Germany

Received December 28, 2007; Revised Manuscript Received January 31, 2008

ABSTRACT: In a quantitative manner, we investigated the mechanism of switching ezrin from the dormant to the active, F-actin binding state by recognition of PIP_2. For this purpose, we established a novel in vitro model mimicking ezrin-mediated membrane−cytoskeleton attachment and compared the F-actin binding capability of ezrin that either had been coupled via a His tag to a lipid bilayer displaying Ni-NTA or had been bound to supported membranes containing PIP_2. Epifluorescence and colloidal probe microscopy (CPM) were employed to demonstrate ezrin's conformational switch into an active conformation capable of binding F-actin. Epifluorescence images revealed attachment of fluorescently labeled F-actin solely to PIP_2-bound ezrin. For the first time, colloidal spheres equipped with an artificial cytoskeleton composed of firmly attached F-actin filaments were used to measure quantitatively the maximal adhesion forces and the work of adhesion of the ezrin−F-actin interface. We found that the work of adhesion between PIP_2-bound ezrin and F-actin is substantially larger than that measured between F-actin and ezrin bound to the membrane via the His tag. Collectively, these data indicate that activation of ezrin can occur as a consequence of PIP_2 binding and does not require additional cofactors.

L-α-Phosphatidylinositol 4,5-bisphosphate (PIP_2)[1] is the major polyphosphate inositide in mammalian cells (*1*). Even though its functions are manifold, PIP_2 comprises only 1% of the phospholipids in the plasma membrane (*2*). Besides its well-known function as a precursor for the two second messengers diacylglycerol and inositol triphosphate, PIP_2 fulfills a number of other functions in the cell (*3*). It is involved in endo- and exocytosis, membrane sorting, enzyme activation, and cytoskeletal attachment. Janmey and Lindberg (*4*) proposed that phosphatidylinositols and Ca^{2+} are the main antagonists in regulating the assembly and disassembly of the cytoskeleton. Raucher et al. (*5*) showed that enzyme-catalyzed hydrolysis of PIP_2 in the plasma membrane decreases considerably the cytoskeleton-to-plasma membrane adhesion energy as monitored by optical tweezers.

Many proteins are indirectly or directly involved in the dynamic processes of membrane−cytoskeleton interaction. In particular ezrin, radixin, and moesin, belonging to the ERM protein family, have been proposed to function as direct linkers between the plasma membrane and F-actin in the cortex of cells. Ezrin is highly expressed in epithelial cells and primarily localized to the apical membrane of such cells. Its structure is characterized by an N-terminal (roughly 300 amino acids) and C-terminal domain (roughly 100 amino acids). The N-terminal domain harbors binding sites for several transmembrane proteins as well as one for PIP_2 (*6*). Mutagenesis experiments within the N-terminal domain revealed that amino acids 63–72 and 253–263 are responsible for PIP_2 binding (*7*). The C-terminal domain contains an F-actin binding site (*8, 9*), which enables the protein to directly link membrane proteins to the actin cytoskeleton. However, in its dormant conformation, both domains are self-associated by a head-to-tail joining that masks the F-actin and membrane protein binding sites, respectively. Activation of ezrin requires separation of the N- and C-terminal domains to expose the N-terminal membrane association site and the C-terminal F-actin binding site. Phosphorylation of T567 (*10, 11*) as well as binding to PIP_2 appears to be crucial for exposing the F-actin binding site. To analyze the synergy between these two events in the conformational activation of ezrin in vivo, Fievet et al. (*12*) made use of mutations abolishing PIP_2 binding and combined these with the activating T567D mutation. They demonstrated that PIP_2 is the primary requirement in the conformational activation of ezrin followed by the threonine phosphorylation. The major role of PIP_2 is also manifested by experiments of Auvinen

[†] Support by the German Science Foundation (SFB 625, DFG Ge514/5-1/2) is gratefully acknowledged.

* Corresponding author. Phone: +49-6131-3923930. Fax: +49-6131-3922970. E-mail: Janshoff@uni-mainz.de.

[‡] University of Mainz.

[§] Georg-August-University of Göttingen.

[||] University of Münster.

[1] Abbreviations: AFM, atomic force microscopy; ATP, adenosine triphosphate; AUT^+, trimethylammonium undecanethiol; C-ERMAD, C-terminal ERM association domain; CPM, colloidal probe microscopy; DOGS-Ni-NTA, 1,2-dioleoyl-*sn*-glycero-3-{[*N*-(5-amino-1-carboxypentyl)iminodiacetic acid]succinyl} Ni salt; DOPC, 1,2-dioleoyl-*sn*-glycero-3-phosphocholine; EDTA, ethylenediaminetetraacetic acid; ERM, ezrin/radixin/moesin; LUV, large unilamellar vesicle; MLV, multilamellar vesicle; N-ERMAD, N-terminal ERM association domain; Ni-NTA, nickel nitrilotriacetic acid; PIP_2, L-α-phosphatidylinositol 4,5-bisphosphate; POPC, 1-palmitoyl-2-oleoyl-*sn*-glycero-3-phosphocholine; SSM, solid-supported membrane; WLC, worm-like chain.

10.1021/bi702542s CCC: $40.75
Published on Web 02/27/2008

et al. (*13*), who showed that overexpression of PIPKα, an enzyme that catalyzes the production of PIP_2, relocates endogenous ezrin partially to the adherens junction, suggesting opening of its dormant state. Compared to other phosphoinositides, the phospholipid $PI(4,5)P_2$ is the important determinant for ezrin binding to the plasma membrane. In contrast to $PI(3,4)P_2$ (<0.15%) and $PI(3,4,5)P_3$ (<0.15%), $PI(4,5)P_2$ represents about 10% of all phosphoinositides in cell membranes (*14*). Only PI(4)P is also found with about 10% in the plasma membrane, but as reported by Niggli et al. (*15*), ezrin is able to discriminate between $PI(4,5)P_2$ and PI(4)P. This has recently been corroborated by Blin et al. (*16*), who showed that the dissociation constant of ezrin bound to PI(4)P is 3–5 times larger than to $PI(4,5)P_2$. They were, moreover, able to demonstrate that the charge density of the membrane is not the decisive parameter for ezrin binding. They showed that, even though the ζ potentials are identical, the K_d values for ezrin binding to $PI(4,5)P_2$ are 16–94 times lower (dependent on the method) than for ezrin bound to phosphatidylserine (PS). The authors also found that the K_d value for $PI(4,5)P_2$ binding remains the same, no matter whether PS is present or not. Together with this information and the ongoing discussion in the literature whether activation of ezrin is driven by a phosphorylation of T567 located in the C-terminus of the protein and/or binding of the N-ERMAD to $PI(4,5)P_2$ embedded in the plasma membrane, we focused our study on $PI(4,5)P_2$-bound ezrin. So far, it has not been investigated whether PIP_2 binding of ezrin alone is able to induce a conformational switch that releases the F-actin binding site.

In this study, we directly addressed this question by a novel in vitro assay and unequivocally show that ezrin is solely activated by PIP_2 embedded in the lipid bilayer. We compared the F-actin affinity of ezrin bound via an N-terminal His tag to Ni-NTA bearing phospholipids with that of ezrin bound to PIP_2-containing solid-supported membranes. For the first time, F-actin-functionalized colloidal probes, which have been invented to measure single particle interactions (*17–19*), were utilized to provide quantitative information about the involved work of adhesion and the signature of force-induced rupture.

EXPERIMENTAL PROCEDURES

Protein Purification. Ezrin was expressed recombinantly in *Escherichia coli* cells [strain BL21(DE3)pLysS] and purified as described previously (*20*) and stored at 4 °C. Protein concentration was determined by UV/vis spectroscopy using an extinction coefficient of $\epsilon_{280} = 66900$ $(M\ cm)^{-1}$.

Vesicle Preparation. Large unilamellar vesicles were prepared according to the extrusion method (*20*). Briefly, multilamellar vesicles (MLVs) composed of POPC/PIP_2 (9:1) or DOPC/DOGS-Ni-NTA (9:1) were obtained by swelling the corresponding lipid films in buffer solution (20 mM Tris-HCl, 50 mM KCl, 2 mM $CaCl_2$, 1 mM NaN_3, pH 7.4) for 30 min and vortexing the suspension three times (30 s every 5 min). MLVs were transformed into large unilamellar vesicles (LUVs) by forcing the vesicle solution through a polycarbonate membrane with 100 nm pore diameters using a miniextruder (LiposoFast, Avestin, Canada).

Supported Bilayer Preparation on Silicon Substrates. Silicon pieces of 1 × 1 cm^2 were cleaned with 2-propanol and water and then placed in a 1% (v/v) aqueous HF solution at room temperature for 15 min to remove the native silicon oxide layer. After being rinsed with water, the hydrophobic silicon was incubated in a $H_2O-NH_4OH-H_2O_2$ (5:1:1) solution at 70 °C for 15 min to form a silicon oxide layer. The substrates were stored under water for a maximum of 1 week and treated with oxygen plasma (Plasma Cleaner, Harrick, NY) for 10 min prior to use. Planar bilayer formation was achieved by incubating with LUVs (0.3 mg/mL) for 1 h and subsequently flushing with 20 mM Tris-HCl, 50 mM KCl, 0.1 mM EDTA, and 1 mM NaN_3, pH 7.4. If bilayers containing DOGS-Ni-NTA were prepared, the same buffer but without EDTA was used for rinsing.

Actin Polymerization. Purified nonmuscle G-actin (monomeric; Cytoskeleton, Denver, CO) was stored at a concentration of 10 mg/mL in 5 mM Tris-HCl, 0.2 mM $CaCl_2$, 0.2 mM ATP, 5% (w/v) sucrose, and 1% (w/v) dextran. Polymerization was achieved by diluting the solution to 1 mg/mL in F-buffer (20 mM Tris-HCl, 50 mM KCl, 2 mM $MgCl_2$, 1 mM ATP, 1 mM NaN_3, pH 7.4) and keeping it at 4 °C overnight.

Ellipsometry. Bilayer formation on silicon substrates and ezrin binding to these bilayers were monitored by time-resolved ellipsometry employing an EL-X-02C (DRE, Ratzeburg, Germany) ellipsometer equipped with a HeNe laser ($\lambda = 632.8$ nm). The angle of incidence of the incoming light was 70°. From the ellipsometric angles Δ and Ψ layer thicknesses of the lipid bilayer and the protein monolayer were calculated by using the following refractive indices for silicon ($n_{Si} = 3.8816$), silica ($n_{SiO_2} = 1.4571$), lipid bilayer ($n_{bil} = 1.4840$), protein ($n_{protein} = 1.5000$), and water ($n_{H_2O} = 1.3328$).

Fluorescence Microscopy. Actin was labeled using 0.05 μM AlexaFluor 488 phalloidin (Invitrogen, Carlsbad, CA). Fluorescence images were obtained with an Axiotech vario microscope (Carl Zeiss GmbH, Göttingen, Germany) equipped with an Achroplan 40×/0.80 w objective. Fluorescence light was detected using filter set 44 (BP 475/40, FT 500, BP 530/50).

CPM: Cantilever Bead Preparation and Functionalization. Silica microspheres (14.5 μm diameter; Bangs Laboratories) were glued with epoxy heat resin (Epikote 1004; Shell) to AFM cantilevers (MLCT, type C, $k \approx 10$ pN/nm, $f_0 \approx 8$ kHz; Veeco, Santa Barbara, CA). After the cantilevers were cleaned with water, 2-propanol, and argon plasma for 60 s, they were coated with 3 nm chromium and 30 nm gold on both sides to prevent them from bending. Afterward, the beads were immersed in a trimethylammonium undecanethiol (AUT^+; ProChimia, Gdansk, Poland) solution (1 mM in 2-propanol) for 12 h followed by rinsing with neat 2-propanol. Finally, the cantilever beads were immersed for 12 h at 4 °C in a 0.02 mg/mL F-actin solution and subsequently washed with F-buffer. Successful functionalization of the colloidal probes was verified by fluorescence microscopy.

AFM/CPM. AFM measurements were carried out with a MFP-3D microscope (Asylum Research, Santa Barbara, CA) at 20 °C in F-buffer (*20*). Only those samples showing complete coverage of the bilayer with ezrin were used for CPM. For CPM measurements, cantilevers were substituted by functionalized colloidal probes. The contact time between

bead and the substrate was set to 1 s before retraction. Load forces did not exceed 200 pN, and no significant impact of the load force on the adhesion forces was measured. The exact spring constants of the cantilevers were determined by the thermal noise method (*21, 22*). A loading rate of 1 nN/s was used throughout all experiments, and the force–distance curves were corrected for hydrodynamic drag as reported elsewhere (*23*).

RESULTS

Using a novel in vitro system for quantitatively analyzing ezrin-mediated membrane−cytoskeleton interactions, we addressed the central question whether binding of ezrin to PIP_2-containing membranes alone leads to a conformational switch, which in turn activates ezrin's F-actin binding capacity. In the dormant state, ezrin is folded in a way that prevents attachment to F-actin, whereas the actin-binding site is accessible in its active state allowing the protein to firmly bind to the actin cytoskeleton. To generate ezrin monolayers in a dormant and a putative active conformation, respectively, ezrin was adsorbed on solid-supported membranes (SSMs) in two different ways. In one scenario, ezrin was attached via an N-terminal His tag to a solid-supported lipid bilayer equipped with Ni-NTA-bearing lipids leading to protein bound in the dormant conformation. In the second scenario, ezrin was bound to a lipid bilayer containing PIP_2.

Ezrin Binding to SSMs. The prerequisite for a quantitative measure of the adhesiveness at the ezrin−F-actin interface in the scenarios outlined above is a complete ezrin monolayer on the solid-supported membrane containing not more than only a small number of defects. Therefore, the formation of supported lipid bilayers and the adsorption of ezrin were monitored by ellipsometry and AFM, providing information on the mesoscopic and microscopic length scale.

To accomplish maximum surface coverage with ezrin, solid-supported membranes equipped with 10 mol % of the receptor lipid (POPC/PIP_2 or DOPC/DOGS-Ni-NTA) were prepared on hydrophilic silicon substrates coated with a thin silicon dioxide layer by fusion of large unilamellar vesicles. The bilayer formation process was followed by ellipsometry as described previously (*24*). A bilayer thickness, as calculated from a readout of Δ and Ψ, of 4–6 nm was obtained, confirming the formation of bilayers with high surface coverage.

Ezrin was applied to the bilayer at a concentration of 0.25–1 μM. This had been shown previously to ensure maximum protein surface coverage on bilayers containing 10 mol % PIP_2 (*20*). Complete coverage is a prerequisite for quantitative colloidal probe experiments, in which the colloidal probe requires to approach a very small area exhibiting complete protein coverage. Hence, we performed all experiments with 10 mol % receptor lipid content to ensure the highest possible surface coverage and as a consequence roughly the same amount of molecular contacts for each force curve. Protein adsorption on the membranes as a function of time was monitored by ellipsometry. If the thickness remained constant, the sample was rinsed with buffer. A mean thickness increase of 2.4 ± 0.8 nm for ezrin bound to PIP_2 and 3.4 ± 0.8 nm for ezrin bound via the His tag to DOGS-Ni-NTA was measured, showing the virtually irreversible adsorption of the protein to the membrane

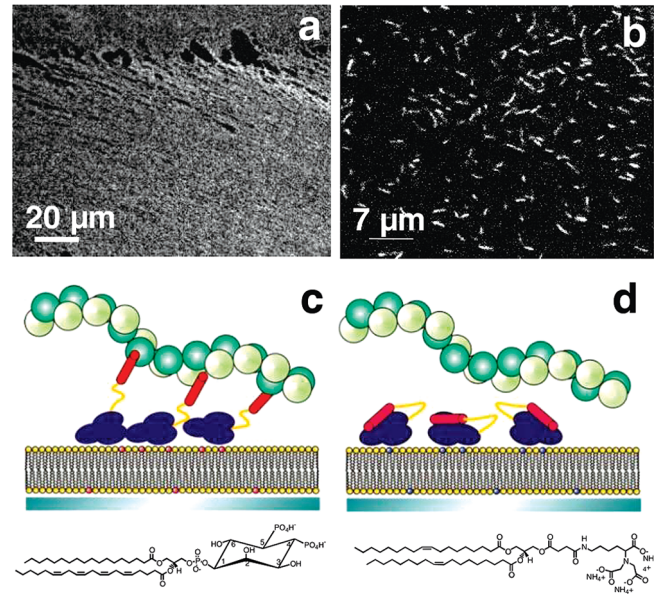

FIGURE 1: (a, b) Fluorescence images of ezrin bound to POPC/PIP_2 (9:1) SSMs incubated with fluorescently labeled F-actin. (c) Schematic drawing of the ezrin activation if bound to PIP_2 (chemical structure below). (d) Scheme illustrating the scenario if ezrin is bound to DOGS-Ni-NTA (chemical structure below), which preserves the dormant state and thus prevents the interaction with F-actin.

surfaces. In both cases, ezrin binding was highly specific; i.e., no nonspecific binding of the protein to pure phosphatidylcholine bilayers was observed.

By means of AFM, we were able to visualize membrane-bound ezrin with very high protein surface coverage on both membrane types. A characteristic height of the protein monolayer of 1.8 ± 0.2 nm (*20*) was obtained for ezrin bound to POPC/PIP_2 membranes. Similar to what had been observed by ellipsometry, we found a slight increase in thickness if ezrin was bound via the His tag to DOPC/DOGS-Ni-NTA membranes (2.5 ± 0.2 nm).

F-Actin Binding to Ezrin Monolayers on SSM. By means of epifluorescence microscopy, the general capability of membrane-bound ezrin to interact with F-actin was investigated. Polymerized F-actin labeled with AlexaFluor 488 phalloidin was added at a concentration of 50 μg/mL to membrane-bound ezrin in F-buffer. After incubation for 2 h, nonbound F-actin was removed by carefully rinsing the surface with F-actin buffer, and fluorescence images were taken. The images clearly reveal that a green fluorescence, originating from F-actin coupled to ezrin, is only observed if ezrin is bound to PIP_2-containing membranes. The surface coverage with F-actin is heterogeneous. While in some areas an almost full coverage with F-actin is observed (Figure 1a), other regions show individual F-actin filaments with an average length of about 1–2 μm (Figure 1b). Control experiments, in which either fluorescently labeled F-actin or only the fluorophor AlexaFluor 488 phalloidin was added to a neat POPC/PIP_2 membrane, showed no detectable fluorescence, demonstrating that nonspecific binding of F-actin and AlexaFluor 488 phalloidin to the membrane can be ruled out (data not shown). Also, no fluorescence was observed if AlexaFluor 488 phalloidin was added to POPC/PIP_2 bilayers with adsorbed ezrin, confirming that the fluorophor itself does not bind to PIP_2-bound ezrin (data not shown). Images obtained from samples, where ezrin was

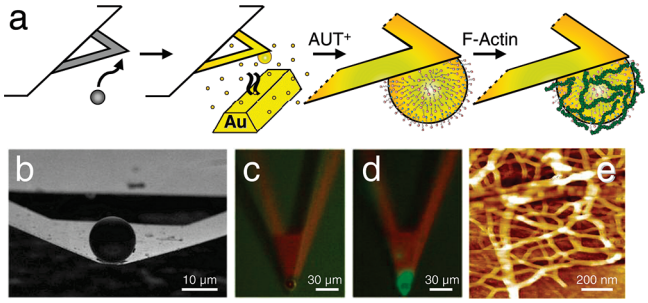

FIGURE 2: (a) Illustration of the preparation and functionalization procedure of cantilever beads. (b) SEM image of a microsphere glued on a cantilever. Fluorescence image of a gold-covered cantilever bead (c) before and (d) after F-actin functionalization. (e) Tapping mode AFM image of actin filaments on AUT$^+$-functionalized mica-stripped gold in F-buffer solution. The filaments exhibit a height of 7 nm.

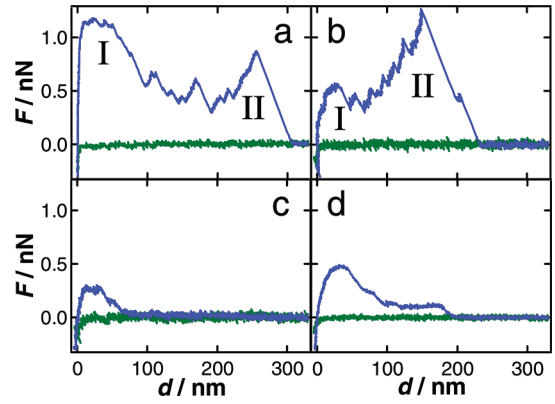

FIGURE 3: Representative force–distance curves (green, trace; blue, retrace) for an F-actin-functionalized cantilever microsphere on various surfaces. (a, b) Ezrin bound to a POPC/PIP$_2$ (9:1) SSM. The curves show generally two pronounced maxima, marked as I and II, including single rupture events in the second force maximum. (c, d) Ezrin associated via the His tag to a DOGS-Ni-NTA-containing bilayer. In general, these curves exhibit only one maximum very close to the surface, followed by a weak long-range attraction at a constant force level, which abruptly breaks off.

bound to the membrane via DOGS-Ni-NTA, did not display any significant fluorescence. Only very rarely were some small fluorescent spots discernible. This suggests that ezrin remains in its dormant conformation in this case and is, thus, incapable of binding F-actin. On average, the mean surface coverage, as obtained from gray scale analyses, was found to be 24 ± 18% for ezrin bound via PIP$_2$ and almost negligible (0.3 ± 0.2%) for ezrin bound via DOGS-Ni-NTA.

CPM and Adhesion Measurements. Adhesion measurements can be carried out with piconewton resolution using an atomic force microscope. Either an AFM tip or a colloidal probe can be approached to and retracted from a surface, resulting in force–distance curves. We found that the yield of successfully functionalized probes was substantially larger if colloidal probes instead of AFM tips were used. The moderate curvature of the spherical colloidal probes as compared to rather sharp AFM tips allows the unperturbed deposition of stiff macromolecules and, thus, provides a more reliable and controllable surface functionalization. With a persistence length of 6–17 μm (*25–28*), F-actin can be considered as a rather stiff, rodlike macromolecule. Moreover, as we were more interested in mimicking the situation of the cytoskeleton attached to the bilayer rather than in the mechanics of individual molecules, F-actin-coated colloidal probes are more suited for this purpose than conventional AFM tips.

Figure 2 summarizes the different preparation steps of functionalized colloidal probes. A microsphere, glued on the cantilever, was gold-covered to allow for chemisorption of positively charged monolayers of trimethylammonium undecanethiol (AUT$^+$). By electrostatic interaction, AlexaFluor 488 phalloidin labeled F-actin was immobilized on the microsphere, which was confirmed by fluorescence microscopy prior each force–distance experiment (Figure 2d). Figure 2e shows an AFM image of actin filaments immobilized on AUT$^+$ on ultraflat (mica-stripped) gold in buffer solution. A network of actin filaments is observed, confirming that the functionalization procedure has been successful. Membrane-bound ezrin was prepared as described above, by adsorbing the protein on planar membranes attached onto silicon dioxide surfaces. AFM images of each preparation step were recorded to ensure a full protein surface coverage prior to the force measurements.

Figure 3 shows typical force–distance curves for colloidal probes functionalized with F-actin touching PIP$_2$-bound ezrin monolayers (panels a and b) and ezrin monolayers coupled via the His tag to DOGS-Ni-NTA-doped SSMs (panels c and d). The retraction curves (blue) display adhesion phenomena caused by an interaction between the F-actin-functionalized colloidal probe and the membrane-bound ezrin. Dependent on how ezrin is bound to the membrane, the retraction curves differ in the maximal force, the number of observed rupture events per curve, and the cumulative work of adhesion, which is obtained by integrating the force–distance curves with respect to the tip–sample distance. Retraction curves obtained from experiments in which ezrin bound via the His tag to DOGS-Ni-NTA was brought in contact with the colloidal probe typically exhibit the maximum adhesion force close to the surface, followed by a weak long-range attraction at a constant force level, which abruptly breaks off when contact of the molecular bridges is lost. In contrast, retraction curves acquired from ezrin monolayers bound via PIP$_2$ to the membrane reveal a large maximum adhesion force in a regime ranging from close to the surface to 100 nm away from it (I) followed by a sawtooth regime with a substantial adhesion peak that extends beyond 100 nm. This signature of force–distance curves upon retraction is not found for ezrin bound via the His tag to the DOGS-Ni-NTA-containing membrane.

The sawtooth pattern in regime II is characterized by prominent force peaks that are reminiscent of protein unfolding events as observed in single molecule stretching experiments (*29*). It is conceivable that in this regime the proteins, most likely ezrin molecules, are stretched until they suddenly unfold and the force immediately decreases as the molecular handle relaxes. In order to verify and support this assumption, single molecule experiments were carried out intentionally using a conventional AFM tip functionalized with F-actin rather than the microsphere retracting from a PIP$_2$-bound ezrin monolayer (Figure 4a). Here, we frequently observed single stretching events as expected for an unfolding of proteins with the typical signature of the nonlinear worm-like chain (WLC) model. Fitting an elastic WLC model to the data provides a persistence length of approximately 0.3–0.4 nm, in good agreement with the typical persistence

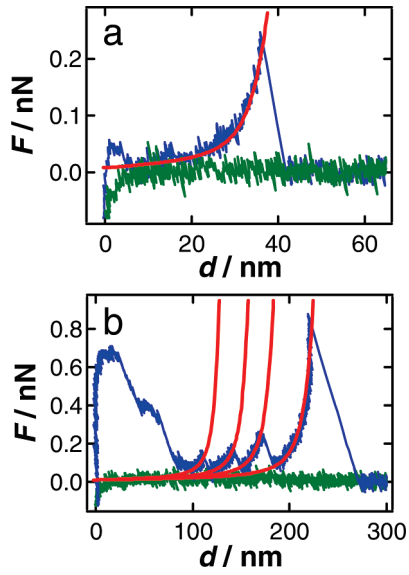

FIGURE 4: Force–distance curves (green, trace; blue, retrace; red, elastic worm-like chain fits) for F-actin-functionalized probes on an ezrin-covered POPC/PIP_2 (9:1) SSM. (a) By using a conventional functionalized AFM tip single nonoverlapping adhesion events with a persistence length of 0.3 nm were observed. (b) By using functionalized microspheres sometimes nonoverlapping peaks could be distinguished, exhibiting a mean persistence length of 0.35 nm, which are attributed to single ezrin−actin rupture events.

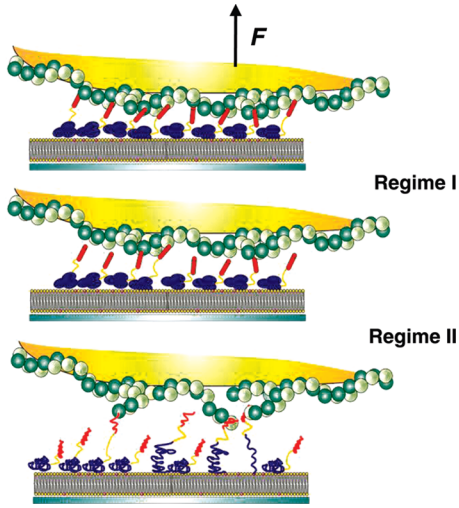

FIGURE 5: Schematic drawing of the adhesion mechanism when retracting a microsphere functionalized with F-actin from an ezrin-covered bilayer containing PIP_2 as the lipid anchor.

length of polypeptide chains (*30*). We used the same model with the same fitting parameters except that we adapted the contour length to describe the sawtooth events we observed in the force–distance curves obtained from functionalized colloidal probes (Figure 4b). The elastic WLC model fits the data well, supporting our hypothesis that in regime II individual ezrin molecules unfold.

Figure 5 envisions the possible scenario that might occur if an F-actin-coated microsphere is separated from a monolayer of activated ezrin molecules bound to PIP_2. Regime I comprises the detachment of the microsphere within the contact area mainly governed by breakage of specific and nonspecific noncovalent bonds (Figure 5a). This leads to a sudden relaxation of the cantilever after the first force maximum (Figure 5b). After relaxation, the remaining bonds between actin and ezrin are stronger than the intramolecular

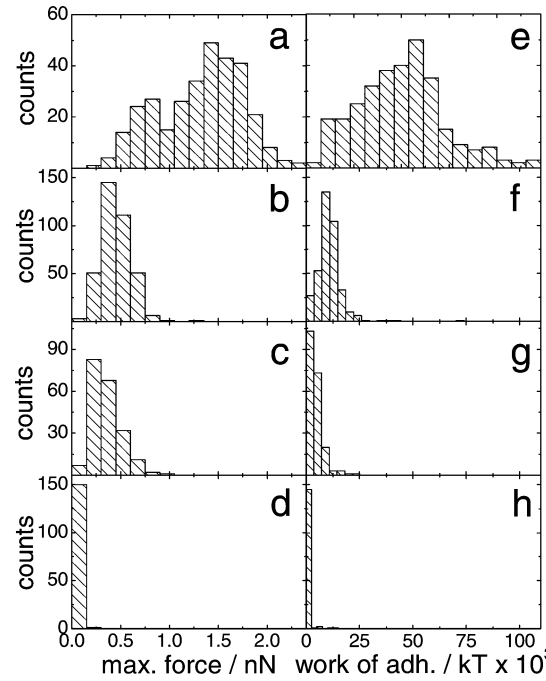

FIGURE 6: Distributions of the maximum adhesion forces (a−d) and the cumulative adhesion energies (e−h) caused by the interaction between F-actin-functionalized microspheres and different surfaces. (a) F-Actin versus PIP_2-bound ezrin ($n = 313$). (b) F-Actin versus DOGS-Ni-NTA-bound ezrin ($n = 369$). (c) Nonfunctionalized microsphere versus PIP_2-bound ezrin ($n = 204$). (d) F-Actin versus POPC/PIP_2 bilayer without ezrin ($n = 151$). (e) F-Actin versus PIP_2-bound ezrin ($n = 313$). (f) F-Actin versus DOGS-Ni-NTA-bound ezrin ($n = 369$). (g) Nonfunctionalized microsphere versus PIP_2-bound ezrin ($n = 204$). (h) F-Actin versus POPC/PIP_2 bilayer without ezrin ($n = 151$).

forces that are responsible for the folded structure of ezrin, which inevitably leads to stretching followed by unfolding of individual proteins that form bridges between the tip and the substrate (Figure 5c). This gives rise to the observed WLC/sawtooth signature in regime II.

The retraction of an F-actin-coated colloidal probe from a monolayer of ezrin bound via the His tag to an SSM does only rarely show stretching events, which can be attributed to unfolding and extension of individual proteins. The signature of adhesion is reminiscent of more typical desorption curves obtained for peeling off polymers attached to a surface (*31*), a behavior that is typically observed for weakly attached macromolecules.

Due to the sharp curvature of the commercial tips, a proper functionalization with F-actin was not highly reproducible, and we refrained from using these cantilevers for a quantitative analysis of the adhesion forces and energies. This is, however, necessary to reveal the differences in binding capability of ezrin adsorbed on either PIP_2- or DOGS-Ni-NTA-containing SSMs. Hence, only experiments with functionalized microspheres were employed to gather quantitative data on the adhesion strength of F-actin attached to surface-bound ezrin.

Adhesion Analysis. We carried out a comprehensive quantitative analysis of adhesion forces and cumulative adhesion energies of F-actin-coated microspheres in contact to monolayers of ezrin attached to either PIP_2- or DOGS-Ni-NTA-containing membranes. Figure 6 summarizes histograms of maximum adhesion forces F_{ad} (Figure 6a−d) and cumulative work of adhesion W_{ad} (Figure 6e−h) found for different

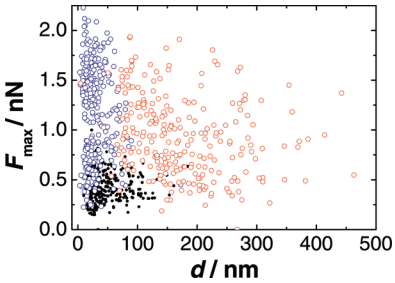

FIGURE 7: Cluster analysis of the force maxima F_{max} as a function of the distance d to the surface. Experiments performed with F-actin versus PIP$_2$-bound ezrin exhibit a force maximum occurring close to the surface (blue circles) with an average maximum force of 1.18 ± 0.48 nN at an average distance of 28.2 ± 19.4 nm. The red circles correspond to dominant force peaks after the first force maximum at greater distances to the surface, exhibiting an average maximum force of 0.94 ± 0.41 nN and a mean distance of 174.7 ± 86.4 nm. Such force peaks are not observed in force–distance curves of F-actin versus DOGS-Ni-NTA-bound ezrin. These curves only exhibit a maximum adhesion force rather close to the surface (black dots) with an average maximum force of 0.45 ± 0.15 nN at a distance of 45.6 ± 30.8 nm.

surface treatments. Noteworthy, the adhesion energies are not free energies since the system is not at equilibrium. Panels a and e of Figure 6 show the results obtained from retracting F-actin microspheres attached to monolayers of ezrin bound to PIP$_2$-containing membranes on silicon. A broad distribution of F_{ad} and W_{ad} with average values of 1.32 ± 0.44 nN and 40 × 10^3 ± 19 × 10^3 kT, respectively, is found. Both average values are significantly larger than those found for experiments in which F-actin microspheres were retracted from an ezrin monolayer bound to DOGS-Ni-NTA-containing bilayers (Figure 6b,f). In this case, F_{ad} amounts to 0.45 ± 0.15 nN and W_{ad} reads only 11 × 10^3 ± 6 × 10^3 kT. Notably, the identical F-actin-functionalized bead was used for both experiments. Moreover, experiments were conducted in reverse order to ensure that weaoff of the actin-coated probe can be ruled out.

Control experiments in the absence of protein–protein interactions employing nonfunctionalized microspheres (Figure 6c,g; F_{ad} = 0.35 ± 0.01 nN, W_{ad} = 4.4 × 10^3 ± 3.3 × 10^3 kT) or a PIP$_2$-doped SSM without bound ezrin (Figure 6d,h; F_{ad} = 0.06 ± 0.01 nN, W_{ad} = 0.3 × 10^3 ± 1.6 × 10^3 kT) resulted in considerably lower adhesion forces and cumulative adhesion energies. For a detailed analysis of the adhesion forces as a function of distance from the surface a cluster analysis was performed. The cluster analysis (Figure 7) visualizes the conceptual differences observed for force–distance curves measured on ezrin monolayers attached either to the membrane via the His tag to DOGS-Ni-NTA lipids or to PIP$_2$. While for PIP$_2$-bound ezrin two force maxima are found, referred to as regimes I (open blue dots) and II (open red dots), only one prominent adhesion peak was usually found if ezrin is bound to DOGS-Ni-NTA (solid black dots). Moreover, if ezrin was bound to PIP$_2$, the maximum adhesion forces for both regimes, I and II, as a function of the tip–sample distance are generally higher. Interestingly, regime I is confined to distances below a tip–sample distance of 100 nm and shows a bimodal distribution, while regime II is spread to tip–sample distances of up to 400 nm and does not exhibit any substructure in the force distribution.

DISCUSSION

Ezrin, as a member of the ERM family, is a multidomain protein providing direct links between the plasma membrane and the actin cytoskeleton. The activation of ERM proteins, resulting in the unmasking of their functional binding sites, is discussed to occur through conformational changes triggered by events including the binding to PIP$_2$ or the Ca^{2+}-regulated protein S100P (*32*) to the N-terminal ERM association domain (N-ERMAD) and the phosphorylation of a conserved threonine in the actin-binding C-ERMAD (T567 in ezrin). The synergy between these two events in the conformational activation of ezrin is, however, still a matter of debate. While ERM proteins phosphorylated at T567 are localized in membrane extensions rich in actin (*33, 34*), experiments using ERM mutants, which should mimic the phosphorylated form, yielded ambiguous results (*35, 36*). In vitro, phosphorylation of the C-ERMAD weakens its interaction with the N-ERMAD (*10, 11*). However, even though phosphorylation appears to be required, it seems not to be sufficient for promoting the association of ERM proteins with F-actin in vitro (*33*). Binding of PIP$_2$ has also been proposed to play an essential role in the conformational activation of ERM proteins. It has been shown that an overexpression of phosphatidylinositol 4-phosphate 5-kinase, responsible for the biosynthesis of PIP$_2$, in mouse fibroblasts and in human HeLa cells results in an accumulation of ezrin at the plasma membrane and at microvillis (*13, 37*). Auvinen et al. (*13*) reported that an upregulation of PIP kinase leads to a colocalization of activated ERM proteins and F-actin. Furthermore, moesin and F-actin cosediment in the presence of PIP$_2$ but not in presence of phosphatidylinositol (*38*). Our experimental in vitro results now provide the direct evidence that PIP$_2$ not only serves as a membrane anchor but in fact is capable of activating ezrin presumably by a conformational switch, which unmasks the F-actin binding site in C-ERMAD. In contrast, ezrin is not able to bind F-actin if the protein is attached to a bilayer via DOGS-Ni-NTA, in agreement with the notion that the protein remains in its dormant conformation.

To elucidate the specific interaction and adhesion of F-actin with membrane-bound ezrin in a more quantitative manner, force–distance measurements were conducted using colloidal probes. Integration of the force–distance curves leads to cumulative adhesion energies that include specific as well as nonspecific interactions between the proteins as well as their elastic behavior. We conclude that the ezrin−actin-specific interactions not only occur very closely to the surface (regime I), partly intermingled with those produced by nonspecific interactions, but predominately take place in regime II (Figure 5).

Regime I is rather unstructured, and it can be assumed that a substantial number of specific and nonspecific bonds are formed within the contact area and ruptured upon pulling. The presence of a second regime (regime II) suggests that bridging occurs between the probe and sample surface that reflects both bending of actin filaments and stretching of proteins, i.e., ezrin.

It is, however, unclear how many bonds are formed and strained in either regime. Parallel bonds enhance the effective binding force not only by the shear addition but also by rendering rebinding more probable as pointed out by Li and

Leckband (*39*). It is conceivable that in the first regime the adhesion force/energy builds up due to many relatively weak parallel bonds that are not sufficiently strong to withstand the unfolding of ezrin molecules. In the second regime only a few but stronger bonds are strained, giving rise to a sawtooth pattern, which can be attributed to stretching (partly in parallel) of polypeptide chains. Proteins such as actin or ezrin being peeled off from the substrate exhibit usually a different signature (*31*), but it might also contribute to the force–distance curve.

Single molecule experiments with conventional AFM tips functionalized with F-actin display forces >100 pN (see Figure 4b), which suggest that around 5–10 bonds are strained in parallel during the CPM experiments. Considering that F-actin is very stiff, exhibiting persistence lengths far beyond 1 μm, and G-actin does not bind to ezrin, it can be concluded that ezrin is unfolded in the second force regime.

From the histogram analysis it is obvious that the adhesion energies as well as the maximum adhesion forces are significantly larger if ezrin is bound via PIP_2 to the lipid bilayer than attached via a His tag. This is consistent with the idea that specific interactions between PIP_2-bound ezrin and F-actin are formed when the colloidal probe comes in contact with the protein monolayer. These specific interactions can only occur if a conformational switch of the protein releases the F-actin binding site at the C-terminus. This hypothesis is further supported by the significant difference in height of the ezrin monolayer depending on the mode of interaction. We found that ezrin attached to PIP_2 displays a smaller height than ezrin bound via the His tag, which is probably the result of the two different conformations.

While scrutinizing the stability of protein–protein interactions in model systems, side effects such as extraction of lipid molecules from the membrane have to be considered. Evans et al. (*40*) determined the extraction forces of single biotinylated lipids from 1-stearoyl-2-oleoylphosphatidylcholine membranes with a biomembrane force probe decorated with streptavidin. With loading rates similar to those used in this study, they measured forces of about 40 pN per lipid. Here, several thousand PIP_2 molecules are underneath the contact radius of the microsphere assuming a molar ratio of POPC/PIP_2 of 9:1 and an average molecular area per lipid of 70 Å^2. Thus, a concerted extraction of several lipid molecules appears to be unlikely. Another possibility could be the detachment of actin filaments from the microsphere. Control experiments performed with F-actin-coated microspheres on an AUT^+-functionalized gold substrate showed the largest observed cumulative work of adhesion ($60 \times 10^3 \pm 16 \times 10^3$ kT). This value is most probably a lower bound for the attachment force between F-actin and an AUT^+-functionalized surface. This is rationalized by the fact that F-actin used for probing is already attached to a positively charged surface; i.e., the gold-covered colloidal probe and thus most of the molecular bonds have already been established, and only a minor amount of attachment sites remain accessible for further binding to the planar AUT^+ surface. Together with the observation that 100–200 force experiments can be carried out without losing binding strength between the ezrin-covered bilayer and the F-actin-functionalized bead, it is very likely that indeed the interaction force between ezrin and F-actin has been measured. Notably, even if the adhesion forces are partly diluted by rupture of weaker F-actin−AUT^+ bonds, it is safe to state that the adhesion forces between ezrin and F-actin are extremely high and activation of the protein by PIP_2 recognition took place.

The strength of the F-actin−ezrin contact is further enhanced by the previously reported attractive lateral intermolecular interactions of ezrin molecules adsorbed on PIP_2-containing bilayers. The ezrin monolayer attached to PIP_2 can be envisioned as a protein carpet that provides additional strength for the cytoskeleton attachment.

ACKNOWLEDGMENT

We thank L. Heim, E. Bonaccurso, and G. Glasser (MPI for Polymer Research, Mainz, Germany) for help to prepare and characterize (SEM) the cantilevers for the CPM experiments.

REFERENCES

1. McLaughlin, S., Wang, J., Gambhir, A., and Murray, D. (2002) PIP_2 and proteins: interactions, organization, and information flow. *Annu. Rev. Biophys. Biomol. Struct. 31*, 151–175.
2. Zahowski, A. (1993) Phospholipids in animal eukaryotic membranes: transverse asymmetry and movement. *Biochem. J. 294*, 1–14.
3. Niggli, V. (2005) Regulation of protein activities by phosphoinositide phosphates. *Annu. Rev. Cell Dev. Biol. 21*, 57–79.
4. Janmey, P. A., and Lindberg, U. (2004) Cytoskeletal regulation: rich in lipids. *Nat. Rev. Mol. Cell Biol. 5*, 658–666.
5. Raucher, D., Stauffer, T., Chen, W., Shen, K., Guo, S., and Meyer, T. (2000) Phosphatidylinositol 4,5 bisphosphate functions as a second messenger that regulates cytoskeleton-plasma membrane adhesion. *Cell 100*, 221–228.
6. Bretscher, A., Edwards, K., and Fehon, R. G. (2002) ERM proteins and merlin: integrators at the cell cortex. *Nat. Rev. Mol. Cell Biol. 3*, 586–599.
7. Barret, C., Roy, C., Montcourrier, P., Mangeat, P., and Niggli, V. (2000) Mutagenesis of the phosphatidylinositol 4,5-bisphosphate (PIP_2) binding site in the NH_2-terminal domain of ezrin correlates with its altered cellular distribution. *J. Cell Biol. 151*, 1067–1080.
8. Gary, R., and Bretscher, A. (1995) Ezrin self-association involves binding of an N-terminal domain to a normally masked C-terminal domain that includes the F-actin binding site. *Mol. Biol. Cell 6*, 1061–1075.
9. Turunen, O., Wahlstrom, T., and Vaheri, A. (1994) Ezrin has a COOH-terminal actin-binding site that is conserved in the ezrin protein family. *J. Cell Biol. 126*, 1445–1453.
10. Matsui, T., Maeda, M., Doi, Y., Yonemura, S. M. A., Kaibuchi, K., Tsukita, S., and Tsukita, S. (1998) Rho-kinase phosphorylates COOH-terminal threonines of ezrin/radixin/moesin (ERM) proteins and regulates their head-to-tail association. *J. Cell Biol. 140*, 647–657.
11. Simons, P. C., Pietromonaco, S. F., Reczek, D., Bretscher, A., and Elias, L. (1998) C-terminal threonine phosphorylation activates ERM proteins to link the cell's cortical lipid bilayer to the cytoskeleton. *Biochem. Biophys. Res. Commun. 253*, 561–565.
12. Fievet, B. T., Gautreau, A., Roy, C., Del Maestro, L., and Mangeat, P. (2004) Phosphoinositide binding and phosphorylation act sequentially in the activation mechanism of ezrin. *J. Cell Biol. 164*, 653–659.
13. Auvinen, E., Kivi, N., and Vaheri, A. (2007) Regulation of ezrin localization by Rac1 and PIPK in human epithelial cells. *Exp. Cell Res. 313*, 824–833.
14. Pendaries, C. (2003) Phosphoinositide signaling disorders in human diseases. *FEBS Lett. 546*, 25–31.
15. Niggli, V., Andreoli, C., Roy, C., and Mangeat, P. (1995) Identification of a phosphatidylinositol-4,5-bisphosphate-binding domain in the N-terminal region of ezrin. *FEBS Lett. 376*, 172–176.
16. Blin, G., Margeat, E., Carvalho, K., Royer, C. A., Roy, C., and Picart, C. (2008) Quantitative analysis of the binding of ezrin to large unilamellar vesicles containing phosphatidylinositol(4,5)-bisphosphate. *Biophys. J. 94*, 1021–1033.

17. Ducker, W. A., Senden, T. J., and Pashley, R. M. (1991) Direct measurement of colloidal forces using an atomic force microscope. *Nature 353*, 239–241.
18. Butt, H.-J. (1991) Measuring electrostatic, van der Waals, and hydration forces in electrolyte solutions with an atomic force microscope. *Biophys. J. 60*, 1438–1444.
19. Kappl, M., and Butt, H.-J. (2002) The colloidal probe technique and its application to adhesion force measurements. *Part. Part. Sys. Charact. 19*, 129–143.
20. Herrig, A., Janke, M., Austermann, J., Gerke, V., Janshoff, A., and Steinem, C. (2006) Cooperative adsorption of ezrin on PIP_2-containing membranes. *Biochemistry 45*, 13025–13034.
21. Butt, H.-J., and Jaschke, M. (1995) Calculation of thermal noise in atomic force microscopy. *Nanotechnology 6*, 1–7.
22. Hutter, J. L., and Bechhoefer, J. (1993) Calibration of atomic-force microscope tips. *Rev. Sci. Instrum. 64*, 1868–1873.
23. Janovjak, H., Struckmeier, J., and Müller, D. J. (2004) Hydrodynamic effects in fast AFM single-molecule force measurements. *Eur. Biophys. J. 34*, 91–96.
24. Faiss, S., Schuy, S., Weiskopf, D., Steinem, C., and Janshoff, A. (2007) Phase transition of individually addressable microstructured membranes visualized by imaging ellipsometry. *J. Phys. Chem. B 111*, 13979–13986.
25. Yanagida, T., Nakase, M., Nishiyama, K., and Oosawa, F. (1984) Direct observation of motion of single F-actin filaments in the presence of myosin. *Nature 307*, 58–60.
26. Gittes, F., Mickey, B., Nettleton, J., and Howard, J. (1993) Flexural rigidity of microtubules and actin filaments measured from thermal fluctuations in shape. *J. Cell Biol. 120*, 923–934.
27. Ott, A., Magnasco, M., Simon, A., and Libchaber, A. (1993) Measurement of the persistence length of polymerized actin using fluorescence microscopy. *Phys. Rev. E 48*, R1642–R1645.
28. Liu, X., and Pollack, G. H. (2002) Mechanics of F-actin characterized with microfabricated cantilevers. *Biophys. J. 83*, 2705–2715.
29. Janshoff, A., Neitzert, M., Oberdörfer, Y., and Fuchs, H. (2000) Force spectroscopy of molecular systems—single molecule spectroscopy of polymers and biomolecules. *Angew. Chem., Int. Ed. 39*, 3346–3374.
30. Rief, M., Gautel, M., Oesterhelt, F., Fernandez, J. M., and Gaub, H. E. (1997) Reversible unfolding of individual titin immunoglobulin domains by AFM. *Science 276*, 1109–1112.
31. Hugel, T., Grosholz, M., Clausen-Schaumann, H., Pfau, A., Gaub, H., and Seitz, M. (2001) Elasticity of single polyelectrolyte chains and their desorption from solid supports studied by AFM based single molecule force spectroscopy. *Macromolecules 34*, 1039–1047.
32. Koltzscher, M., Neumann, C., König, S., and Gerke, V. (2003) Ca^{2+}-dependent binding and activation of dormant ezrin by dimeric S100P. *Mol. Biol. Cell 14*, 2372–2384.
33. Nakamura, F., Amieva, M. R., Hirota, C., Mizuno, Y., and Furthmayr, H. (1996) Phosphorylation of T-558 of moesin detected by site-specific antibodies in RAW264.7 macrophages. *Biochem. Biophys. Res. Commun. 226*, 650–656.
34. Hayashi, K., Yonemura, S., Matsui, T., and Tsukita, S. (1999) Immunofluorescence detection of ezrin/radixin/moesin (ERM) proteins with their carboxyl-terminal threonine phosphorylated in cultured cells and tissues. *J. Cell. Sci. 112*, 1149–1158.
35. Gautreau, A., Louvard, D., and Arpin, M. (2000) Morphogenic effects of ezrin require a phosphorylation-induced transition from oligomers to monomers at the plasma membrane. *J. Cell Biol. 150*, 193–204.
36. Chambers, D. N., and Bretscher, A. (2005) Ezrin mutants affecting dimerization and activation. *Biochem. Int. 44*, 3926–3932.
37. Matsui, T., Yonemura, S., and Tsukita, S. (1999) Activation of ERM proteins in vivo by Rho involves phosphatidyl-inositol-4-phosphate 5-kinase and not ROCK kinases. *Curr. Biol. 9*, 1259–1262.
38. Huang, L., Wong, T. Y., Lin, R. C., and Furthmayr, H. (1999) Replacement of threonine 558, a critical site of phosphorylation of moesin in vivo, with aspartate, activates F-actin binding of moesin. Regulation of conformational changes. *J. Biol. Chem. 274*, 12803–12810.
39. Li, F., and Leckband, D. (2006) Dynamic strength of molecularly bonded surfaces. *J. Chem. Phys. 125*, 194702.
40. Evans, E., and Ludwig, F. (2000) Dynamic strengths of molecular anchoring and material cohesion in fluid biomembranes. *J. Phys. Condens. Matter 12*, A315–A320.

BI702542S